Optics and Lasers in Engineering 160 (2023) 107306

Contents lists available at ScienceDirect

Optics and Lasers in Engineering

journal homepage: www.elsevier.com/locate/optlaseng

Interferenceless incoherent digital holography with binary coded apertures optimized using direct binary search

Manoj Kumar[a,b,*], Vijayakumar Anand[a,b], Joseph Rosen[a]

[a] School of Electrical and Computer Engineering, Ben-Gurion University of the Negev, P.O. Box 653, Beer-Sheva 8410501, Israel
[b] Institute of Physics, University of Tartu, W. Ostwaldi 1, 50411 Tartu, Estonia

ARTICLE INFO

Keywords:
Digital holography
Imaging systems
Computer holography
Coded aperture
Diffraction and gratings

ABSTRACT

Coded aperture correlation holography offers 3D imaging with improved lateral and axial resolutions. This study is an additional advancement in the line of imaging systems with a pseudorandom coded aperture. Starting with the coded aperture correlation holography system implemented on an incoherent on-axis interferometer, we proposed interferenceless and lensless versions of the system. In the present study, we propose replacing the multi-values phase aperture mask with a binary mask. Two binary masks synthesized iteratively are used in two camera shots. Each mask is obtained from an iterative optimization process known as direct binary search, where the optimized cost function is the peak-to-background ratio of a reconstructed point object. Overall, the system demonstrates a lower background noise compared to other methods, enabling 3D imaging capability with only two camera shots, a substantial improvement in comparison to the many shots in the original systems. Using binary masks might extend the usefulness of the coded aperture holography for new regions in the electromagnetic spectrum other than the visual band, as of X-ray and THz bands.

1. Introduction

Incoherent digital holography systems have come into prominence because of the several advantages they possess over their coherent counterparts, such as improved resolution capabilities due to the higher spatial bandwidth of incoherent imaging systems and the capability to image 3D scenes illuminated by natural light and self-luminance objects [1–6]. Moreover, the incoherent light sources are used to avoid edge ringing effects and speckle noise during imaging [7–9]. In view of this, various incoherent digital holography techniques have been developed [1-6,10]. An incoherent digital holography technique termed Fresnel incoherent correlation holography (FINCH) was developed based on the self-reference holography principle and demonstrated a possibility of achieving improved lateral resolution in comparison to other equivalent imaging systems [2,10,11]. The optimal FINCH system exhibits a lateral resolution 2 times and 1.5 times higher than that of equivalent coherent and incoherent imagers, respectively [11]. However, the axial resolution of FINCH is relatively lower. Recently, another self-informative-reference holography technique called coded aperture correlation holography (COACH) was developed to solve the axial resolution limitation of FINCH at the expense of loss of some lateral resolution [12]. COACH has the same axial and lateral resolutions as that of a regular lens-based imaging system with the same numerical aperture (*NA*) but with 3D imaging capability that does not exist with a single camera shot captured by a regular system. In both COACH and FINCH, the light from each object point is split into two mutually coherent beams. One beam is modulated by a coded phase mask (CPM), while another beam remains unmodulated. The modulated and unmodulated beams interfere, and the interference pattern is recorded by a camera. The recorded hologram contains the 3D information of the object. In FINCH, the CPM is a 2D quadratic phase function whereas, in COACH, the CPM is a pseudorandom phase function.

Different noise reduction techniques such as phase-only filtering and averaging were implemented to reduce the background noise in the reconstructed images and to enhance the performance of COACH [13]. A modified version of COACH for 4D imaging of objects at the three spatial dimensions and with an additional spectral dimension using a diffractive objective lens has been reported [14]. Further advancement in the COACH system has been done by developing the interferenceless COACH (I-COACH), in which the hologram is recorded without two-wave interference [15]. In COACH and I-COACH, a pseudorandom CPM is used with which chaotic amplitude and phase distributions are obtained on the camera plane. Thus, the 3D information of the object is encoded not only in the phase of the diffracted wave, as is the case in FINCH, but also in the amplitude. Therefore, two-wave interference is not necessary to retrieve the 3D information of the object. Moreover, the drawbacks associated with interference-based holographic systems, e.g., the requirement of high optical power, equalizing the power of in-

* Corresponding author.
E-mail address: manojklakra@gmail.com (M. Kumar).

https://doi.org/10.1016/j.optlaseng.2022.107306
Received 5 July 2022; Received in revised form 14 September 2022; Accepted 23 September 2022
Available online 12 October 2022
0143-8166/© 2022 Elsevier Ltd. All rights reserved.

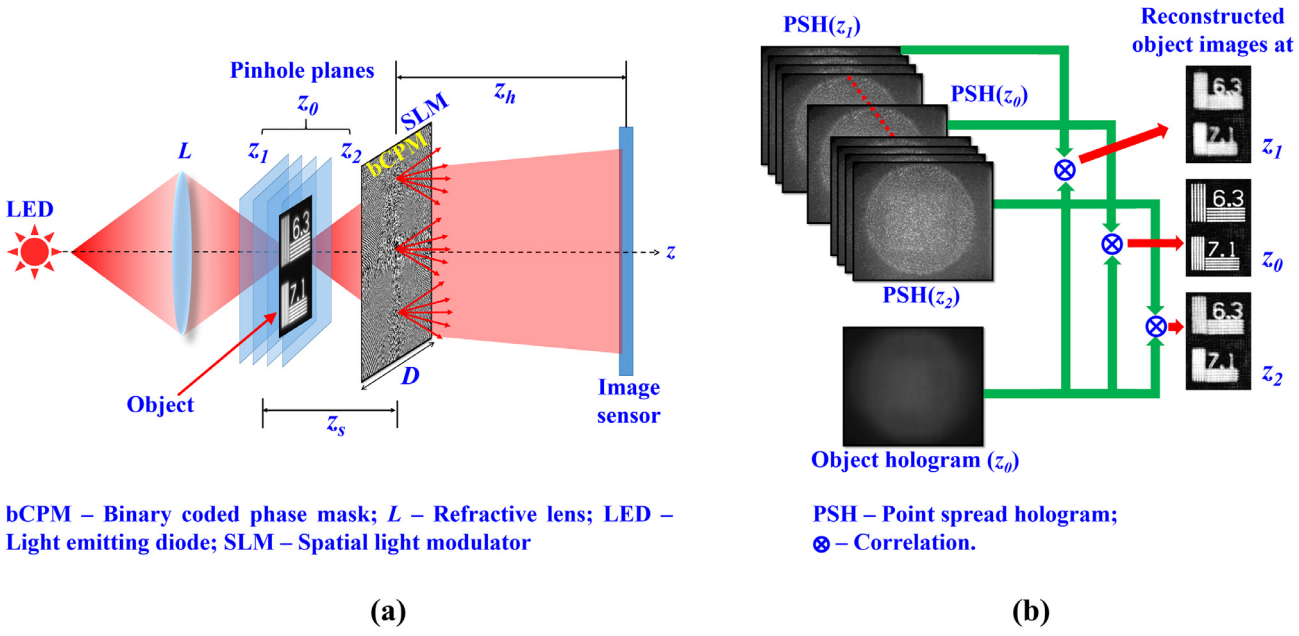

Fig. 1. (a) Optical configuration of LI-COACH and (b) object reconstruction procedure from the recorded PSH library and the object hologram.

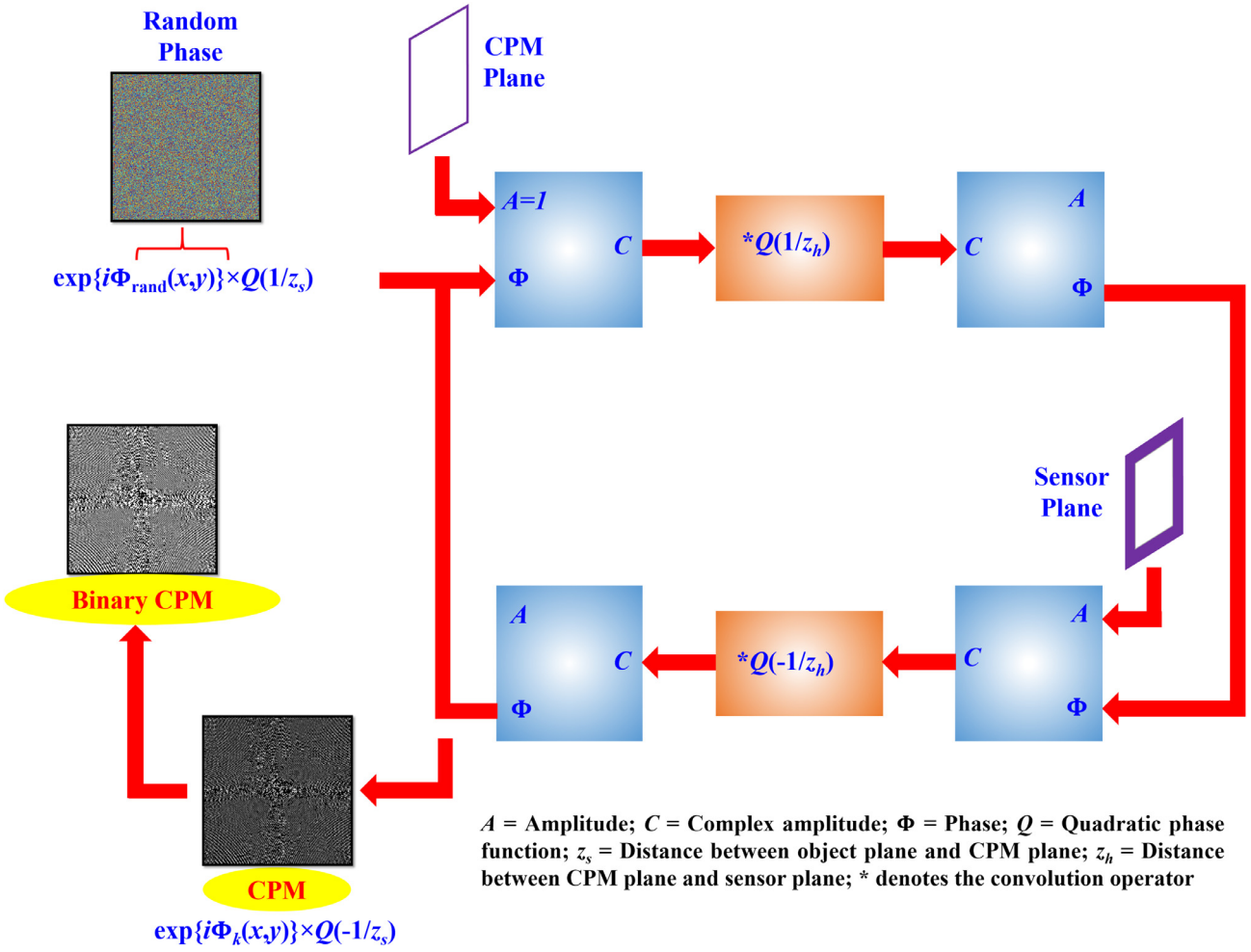

Fig. 2. Block diagram of GSA to calculate the initial binary coded mask.

terfering beams, time-consuming optical alignment procedures, vibration isolation systems, and high temporal coherence, can be avoided in I-COACH. The performances, including the axial and lateral resolutions of I-COACH, are similar to that of COACH [15].

Recently, a lensless I-COACH (LI-COACH) without refractive lenses and with a simpler optical configuration was reported [16]. In LI-COACH, the 3D information of the incoherently illuminated object is recorded and stored onto a 2D hologram without using wave interference and any refractive lens. Furthermore, the hologram is acquired with only two camera shots in contrast to I-COACH, which requires three camera shots. Therefore, LI-COACH can be considered a powerful 3D imaging technique that can be exploited for imaging in even other regimes of the electromagnetic spectrum, such as X-rays, for instance, where the fabrication of lenses is a difficult or expensive task. Coded aperture imaging has been proven as an effective technique in X-ray cameras and telescopes [17], gamma-ray imagers for medical applications [18], explosive detection [19], and non-destructive techniques [20]. In spite of all the above-mentioned advantages, the need for a coded aperture with a multi-level pseudorandom phase profile imposes a strict constraint for real applications. In [16], the LI-COACH has been demonstrated using a spatial light modulator (SLM) as the display for CPM. However, for applications in other electromagnetic regimes or telescopic imaging applications, the fabrication of a pseudorandom phase profile might be a challenging task. Another disadvantage of LI-COACH is the low signal-to-noise ratio (SNR) present during reconstruction and the need for averaging [13] several images obtained by different independent pseudorandom phase masks. Such an averaging process slows the acquisition process of images in LI-COACH.

In this study, we address two problems: 1. manufacturing difficulties of CPM with multi-level phase values, and 2. the need for averaging the reconstructed images using multiple CPMs and consequently reducing the time resolution. In order to solve the first problem, we propose to use binary CPM as the aperture in the LI-COACH system. To solve the second problem of relatively high background noise, we suggest a two-step hybrid iterative algorithm combining the Gerchberg-Saxton algorithm (GSA) and direct binary search algorithm (DBSA) for synthesizing the final binary CPM. The DBSA has already been proven to be a powerful tool for computer-generated holograms and as an efficient optimization process yielding solutions that are relatively close to the global optimum [21–25]. Hence, it is expected from the DBSA to synthesize CPMs that are capable of reconstructing 3D images with a higher SNR than the former used GSA. In this study, a relatively slow DBSA is modified to enable faster synthesis of the binary CPMs, and the cost function of the DBSA has been selected to achieve high SNR.

The next section describes the theoretical analysis and the methodology. In the third section, the experimental procedure and the results are described, followed by the discussion in the final section.

2. Methodology

The optical configuration of LI-COACH for recording the object hologram and point spread hologram (PSH) is shown in Fig 1(a), and the procedure of 3D image reconstruction using the PSH library is demonstrated in Fig 1(b). A quasi-monochromatic light source is used to illuminate a point object (a pinhole) using a refractive lens *L*. The light diffracted by the object is modulated by a pseudorandom binary CPM. The initial non-binary version of the CPM is synthesized by modified GSA [16,26] with Fresnel propagation from the CPM plane to the image sensor and back. In order to reduce the background noise during reconstruction, the constraint on the camera plane is set to create a function with a uniform magnitude on a predefined area. After passing through a pinhole placed at a distance z_s from the CPM, the light is scattered by the CPM and recorded by the image sensor on which the difference between two detected intensity patterns (with two different CPMs) is the PSH. An object is placed at the same axial location as the point object, and the intensity pattern called the object hologram is also the difference between two recorded patterns obtained with the same CPMs and under identical conditions. Using two recorded intensity patterns corresponding to two different independent CPMs is done to improve the SNR in the reconstructed image of the object [16]. In other words, the final PSH and object hologram is synthesized as the difference between the two independent intensity patterns recorded by the image sensor, and this process is carried out for each element of the PSH library. The image of the object is reconstructed by cross-correlating the object hologram with the PSH. To reconstruct a multiplane or 3D object, a library of PSHs at all possible axial locations is required. The library of PSHs is created by shifting the pinhole along all possible axial locations and recording the corresponding intensity patterns. An object is placed within the axial boundaries of the PSH library and the intensity pattern of the object is recorded. The different planes of the object are reconstructed by correlating the corresponding PSHs from the library. It must be noted that this process of creating the PSH library needs to be done only once and can be used any number of times for reconstructing objects. The object reconstruction procedure from the recorded PSH library and the object hologram is shown in Fig 1(b).

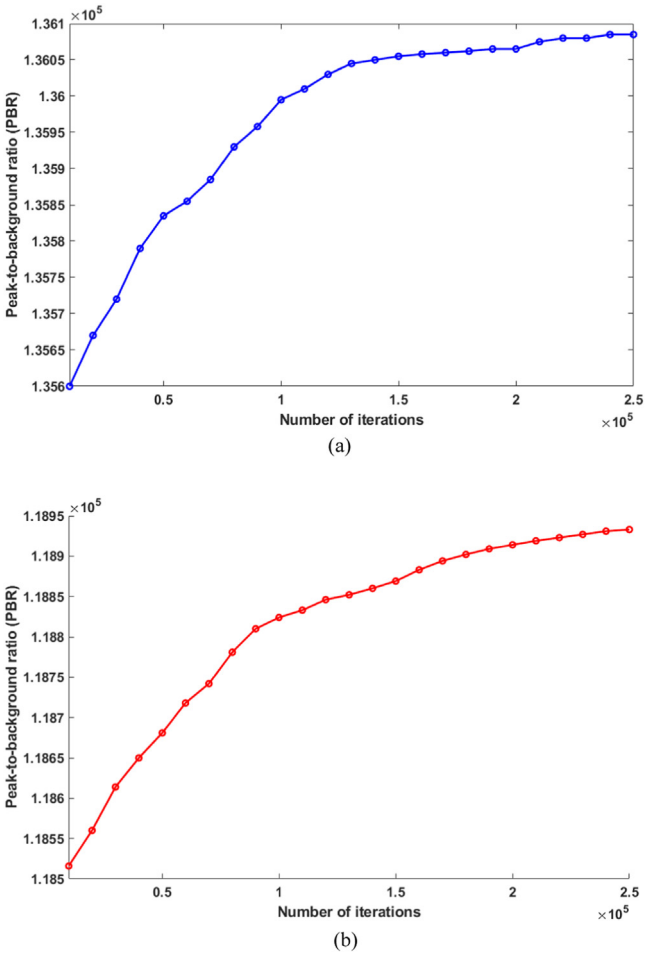

Fig. 3. Plot of PBR versus the number of iterations for (a) the Fast DBSA method and (b) the FFT-based DBSA method.

Fig. 2 shows the block diagram of the GSA for generating the initial mask of the binary CPM before using the DBSA for computing the final CPM. First, a random phase $\Phi(x,y)$ is generated and multiplied with a diverging spherical wave originating from a point object located on the optical axis at a distance z_s from the CPM. The phase distribution is extracted from the complex amplitude obtained after propagating from the CPM to the sensor plane. The sensor plane is located at a distance z_h from the CPM plane, and hence the complex amplitude

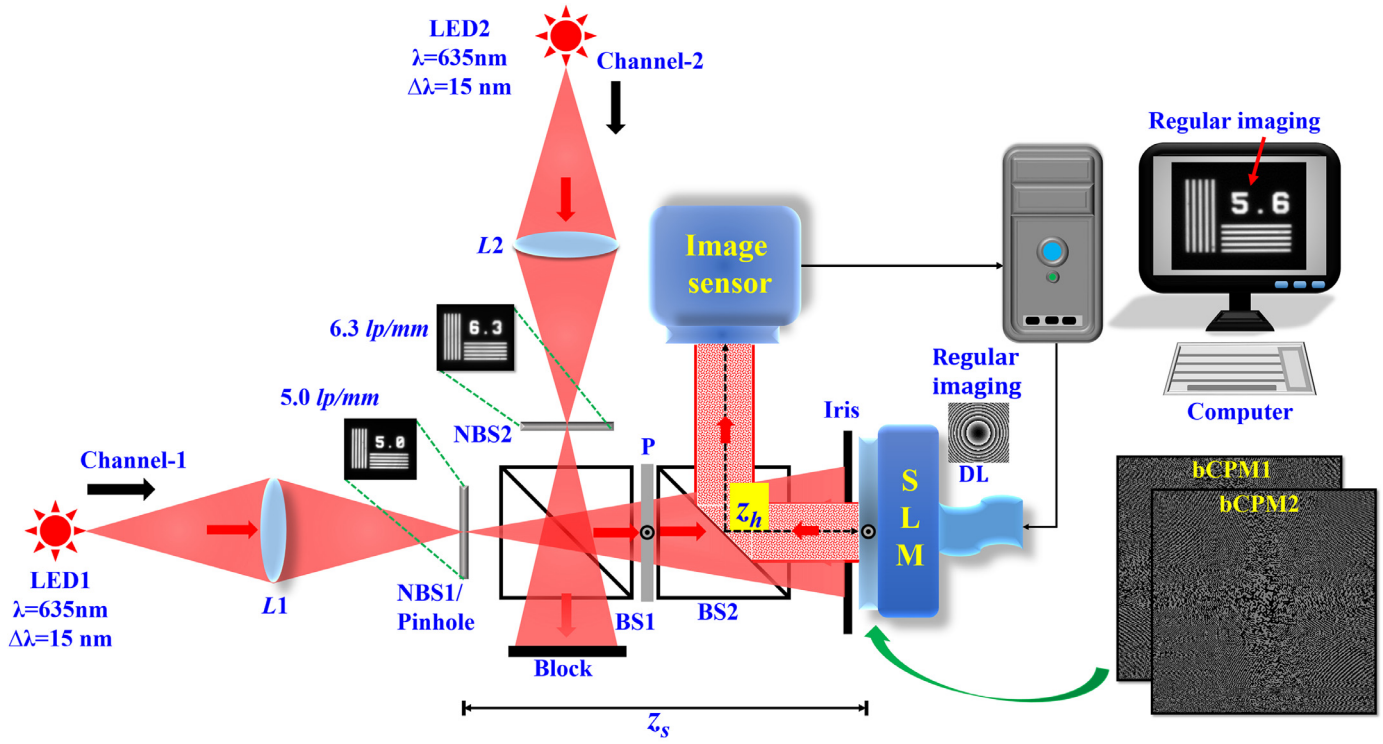

BS1, BS2 – Beam splitters; bCPM1, bCPM2 – Binary coded phase masks; DL – Diffractive lens; *L*1, *L*2 – Refractive lenses; LED1, LED2 – Light emitting diodes; NBS1, NBS2 – National bureau of standards; P – Polarizer; SLM – Spatial light modulator; ⊙ – Polarization orientation perpendicular to the plane of the page

Fig. 4. Experimental setup of LI-COACH with two illumination channels.

on the sensor plane is a 2D convolution between the complex amplitude beyond the CPM and the Fresnel free-space kernel $Q(1/z_h)$ given as $Q(1/z_h) = \exp[i\pi(z_h\lambda)^{-1}(x^2+y^2)]$.The magnitude is replaced by a zero-padded uniform matrix in order to get a uniform intensity distribution over a predefined area at the center of the sensor plane. The resulting complex amplitude at the sensor plane is back propagated to the CPM plane using the Fresnel back propagation [Convolution with $Q(-1/z_h)$], and the phase of the complex amplitude is extracted and attached to a constant magnitude for the next iteration. This cycle is repeated until the generated intensity profile at the sensor plane converges towards the constraint. The obtained phase from GSA is multiplied by $Q(-1/z_s)$ in order to cancel the effect of the initial input spherical wave phase $Q(1/z_s)$.

The following mathematical analysis of LI-COACH is based on the experimental setup in Fig 1(a). The light diffracted from a point object located at $(\bar{r}_s, z_s) = (x_s, y_s, z_s)$, with an amplitude of $\sqrt{I_s}$, reaches the CPM with a complex amplitude $\sqrt{I_s}C_1 L(\bar{r}_s/z_s)Q(1/z_s)$, where C_1 is a complex constant, L and Q represent linear and quadratic phase functions, given by $L(\bar{s}/z) = \exp[i2\pi(\lambda z)^{-1}(s_x x + s_y y)]$ and $Q(a) = \exp[i\pi a\lambda^{-1}(x^2+y^2)]$, respectively. The complex amplitude after the CPM is given by $\sqrt{I_s}C_1 L(\bar{r}_s/z_s)Q(1/z_s)\exp[i\Phi_k(\bar{r})]$, where $\Phi_k(\bar{r})$ is the k-th quasi-random phase of the CPM calculated using the modified GSA. The complex amplitude at the image sensor is obtained as a result of the convolution of $\sqrt{I_s}C_1 L(\bar{r}_s/z_s)Q(1/z_s)\exp[i\Phi_k(\bar{r})]$ with $Q(1/z_h)$, where $\Phi_k(\bar{r}) \in \{0, 2\pi\}$. Therefore, the k-th intensity pattern on the image sensor is given by,

$$I_k(\bar{r}_0; \bar{r}_s, z_s) = \left|\sqrt{I_s}C_1 L\left(\frac{\bar{r}_s}{z_s}\right) Q\left(\frac{1}{z_s}\right)\exp\left[i\Phi_k(\bar{r})\right] * Q\left(\frac{1}{z_h}\right)\right|^2 = I_k\left(\bar{r}_0 - \frac{z_h}{z_s}\bar{r}_s; 0, z_s\right) \quad (1)$$

where the asterisk sign denotes a two-dimensional convolution and $\bar{r}_0 = (u, v)$ is the transverse location vector on the sensor plane. The intensity on the sensor plane is a shifted version of the intensity response for a point object located on the optical axis ($\bar{r}_s = 0$) and is represented by the second equality of Eq. (1), where the distance of the shift is $\bar{r}_s z_h/z_s$. This last equality of Eq. (1) is valid in the paraxial approximation as long as the free-space propagation is expressed by convolution of the input complex amplitude with quadratic phase kernel. The validation of this intensity shift and the shift value can be easily obtained by a variable exchange inside the free-space convolution integral.

A 2D object placed at a distance of z_s from the SLM can be considered as a collection of M object points given by

$$o(\bar{r}_s) = \sum_j^M a_j \delta(\bar{r} - \bar{r}_{s,j}) \quad (2)$$

When the object is illuminated by an incoherent quasi-monochromatic light source, there is no interference between the various responses of the form given by Eq. (1). Hence, the overall intensity distribution on the sensor plane is a sum of the individual responses of the different object points, given by,

$$I_{OBJ,k}(\bar{r}_0; z_s) = \sum_j^M a_j I_k\left(\bar{r}_0 - \frac{z_h}{z_s}\bar{r}_{s,j}; 0, z_s\right) \quad (3)$$

Both $I_{OBJ,k}(\bar{r}_0; z_s)$ and $I_k(\bar{r}_0; z_s)$ are real positive chaotic distributions. The image of the object can be reconstructed by a cross-correlation between the intensity response to a point $I_k(\bar{r}_0; z_s)$ and the intensity response to the object, $I_{OBJ,k}(\bar{r}_0; z_s)$. The cross-correlation between two real positive functions gives undesired background noise over the reconstructed image. In order to minimize the noise, the autocorrelation of the PSH should be as close as possible to the δ function. From the convolution theorem, this condition can be satisfied if the magnitude of the Fourier transform of the PSH is uniform and equal to some constant greater than zero. This property cannot be achieved

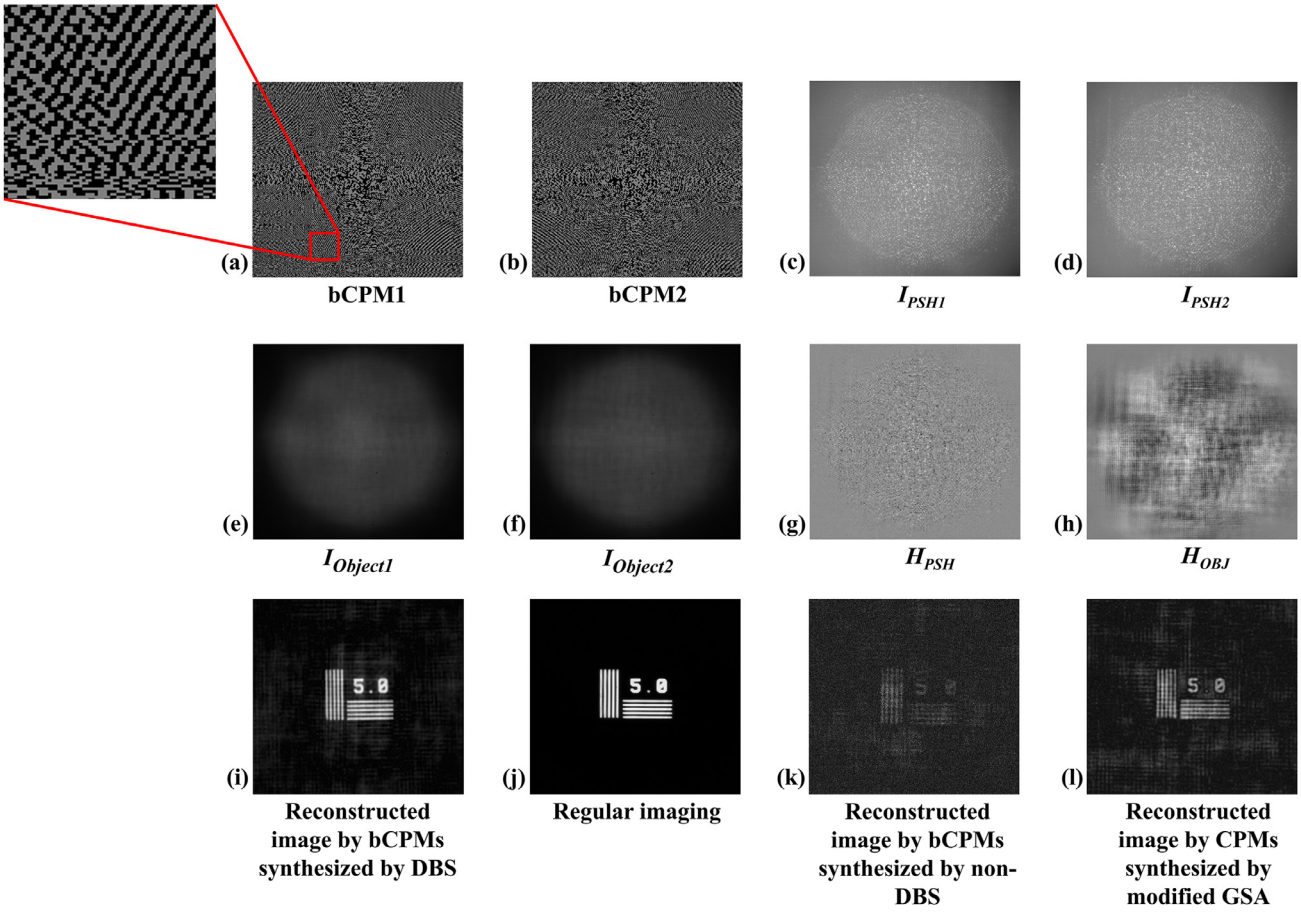

Fig. 5. (a), (b) Binary CPMs: bCM1 and bCM2; (c), (d) intensity patterns of PSHs corresponding to bCM1 and bCM2, respectively; (e), (f) intensity patterns of object holograms corresponding to bCM1 and bCM2, respectively; (g), (h) magnitude of the hologram of the pinhole and the NBS1 RC; (i) reconstructed image after DBSA; (j) regular imaging; (k) reconstructed image by initial bCPMs without DBSA; and (*l*) reconstructed image by multilevel CPMs synthesized by modified GSA. Image size (a-h) is 1080×1080 pixels^2 and (i-l) is 940×800 pixels^2.

with real positive PSH because of the value at the origin of the spectrum (the zero-diffraction order, which is equal to the integral over the real positive PSH), which is more intense than any other value. Only a superposition of $K \geq 2$ intensity responses can minimize the bias value of the PSH and approximately satisfy the constraint of the uniform spectrum. To minimize the number of camera shots, in this study, we use the minimum value $K = 2$. Therefore, to minimize the background noise, the PSH $[H_{PSH}(\bar{r}_0; z_s)]$ is calculated as follows,

$$H_{PSH}(\bar{r}_0; z_s) = I_1(\bar{r}_0; z_s) - I_2(\bar{r}_0; z_s) \tag{4}$$

A further noise reduction is achieved when the object hologram is cross-correlated with a version of the PSH that its Fourier transform is a phase-only filter (POF) [13]. Therefore, the PSH is Fourier transformed, and only its phase profile is extracted and used in the spatial filtering process.

Similarly, two intensity patterns are recorded for the object using the same two CPMs used for synthesizing the PSH.

$$\begin{aligned} &H_{OBJ}(\bar{r}_0; z_s) = I_{OBJ,1}(\bar{r}_0; z_s) - I_{OBJ,2}(\bar{r}_0; z_s) \\ &= \sum_j^M a_j I_1\left(\bar{r}_0 - \tfrac{z_h}{z_s}\bar{r}_{s,j}; 0, z_s\right) - \sum_j^M a_j I_2\left(\bar{r}_0 - \tfrac{z_h}{z_s}\bar{r}_{s,j}; 0, z_s\right) \\ &= \sum_j^M a_j H_{PSH}\left(\bar{r}_0 - \tfrac{z_h}{z_s}\bar{r}_{s,j}; z_s\right), \end{aligned} \tag{5}$$

The image is reconstructed by correlating $H_{OBJ}(\bar{r}_0; z_s)$ with the POF of $H_{PSH}(\bar{r}_0; z_s)$ as follows,

$$\begin{aligned} &P(\bar{r}_R) = \int\int H_{OBJ}(\bar{r}_0; z_s)\tilde{H}^*_{PSH}(\bar{r}_0 - \bar{r}_R; z_s)d\bar{r}_0 \\ &= \int\int \sum_j a_j H_{PSH}\left(\bar{r}_0 - \tfrac{z_h}{z_s}\bar{r}_{s,j}; z_s\right)\tilde{H}^*_{PSH}(\bar{r}_0 - \bar{r}_R; z_s)d\bar{r}_0 \\ &= \sum_j a_j \Lambda\left(\bar{r}_R - \tfrac{z_h}{z_s}\bar{r}_{s,j}\right) \approx o\left(\tfrac{\bar{r}_s}{M_T}\right). \end{aligned} \tag{6}$$

where $\tilde{H}_{PSH}(\bar{r}_0; z_s) = \mathfrak{F}^{-1}\left\{\exp\left[i \cdot \arg\left(\mathfrak{F}\left\{H_{PSH}(\bar{r}_0; z_s)\right\}\right)\right]\right\}$ and $\mathfrak{F}$, $\mathfrak{F}^{-1}$ stand for 2D Fourier and inverse Fourier transforms, respectively. Λ is a δ-like function, $\sim$1 at (0,0) and $\sim$0 elsewhere. Since the image is reconstructed by a cross-correlation, the transverse and axial resolutions are governed by the transverse and axial correlation lengths, determined by the width and the length of the smallest spot that can be recorded on the sensor plane by the SLM with an active area of a diameter of D. Therefore, the transverse and axial resolutions are approximately $1.22\lambda z_s/D$ and $8\lambda(z_s/D)^2$, respectively, results that are the same as that of regular imaging with the same NA. The magnification of the imaging system is implied from Eq. (6) in $M_T = z_h/z_s$.

Returning to the original problem of synthesizing a binary CPM (bCPM) with reduced background noise, we present the following procedure. The phase of CPM obtained from the modified GSA, described in Fig 2, was converted into an initial binary phase distribution $\Phi_k(\bar{r}) \in \{0, a\}$ for the DBSA, where $a = 0.6\pi$ *Rad*. The phase value 0.6π is chosen

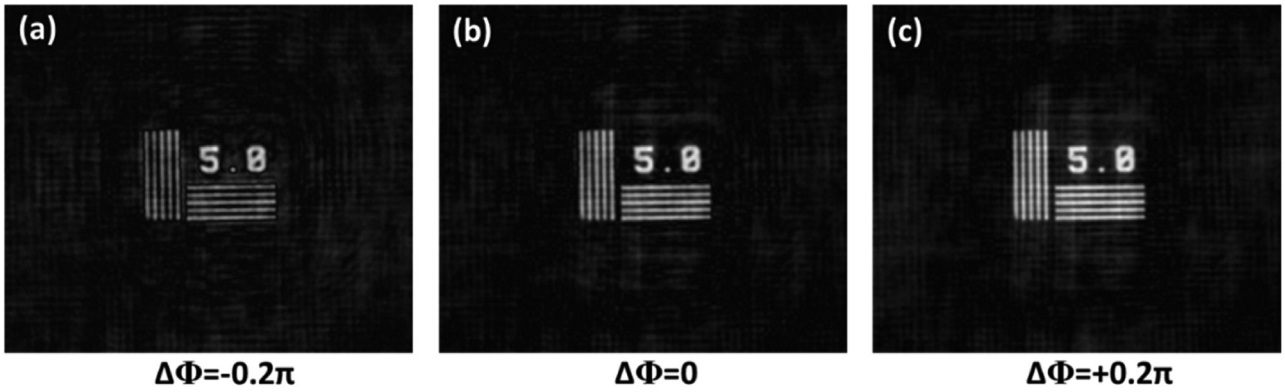

Fig. 6. Reconstruction results with a phase error of (a) $\Delta\Phi = -0.2\pi$, (b) $\Delta\Phi = 0$ and (c) $\Delta\Phi = +0.2\pi$. Image size (a-c) is 940 × 800 pixels^2.

according to the desired size of the PSH on the camera plane. The conversion formula from the multilevel phase to the initial bCPM is: Φ=0 for $0.3\pi \geq \Phi \geq -0.7\pi$ and 0.6π otherwise. The bCPM is changed by the DBSA with the goal of achieving the highest SNR. Two different bCPMs were synthesized from two different initial random phase profiles using the modified GSA and the image of the point object was reconstructed as the autocorrelation of the PSH given by

$$P(\bar{r}_R) = \int\int H_{PSH}(\bar{r}_0; z_s)\tilde{H}^{*}_{PSH}(\bar{r}_0 - \bar{r}_R; z_s)d\bar{r}_0 = \Lambda(\bar{r}_R) \quad (7)$$

The peak-to-background ratio (PBR) of the reconstructed point image with an intensity profile $P(\bar{r}_R)$ is defined as

$$PBR(m) = \frac{\left|P_m(\bar{r}_R = (0,0))\right|}{N^{-2}\sum_{x,y=-N/2}^{x,y=N/2}\left|P_m(\bar{r}_R)\right|} \quad (8)$$

and is used as the cost function maximized by the DBSA. The parameter m is the iteration number of the DBSA. In this procedure, the binary phase profile of one of the bCPMs ($bCPM_1$) is kept static while the other bCPM ($bCPM_2$) is varied. The PBR is evaluated for every m^{th} iteration up to a total of M iterations which completes one cycle consisting of $M = N \times N$ operations, where N is the number of rows and columns of the bCPM matrices. The phase profile of $bCPM_2$ is scanned pixel by pixel in lexicographic order and every pixel of the binary pattern is toggled between 0 and a phase value of 0.6π Rad. The updated mask $bCPM_2(m+1)$ is used to synthesize the PSH$(m+1)$, which is introduced to Eqs. (7) and (8) for updating the PBR$(m+1)$ and comparing it with PBR(m). If the PBR$(m+1) \geq$PBR(m), $bCPM_2(m+1)$ is retained. Otherwise, $bCPM_2$ is flipped back to $bCPM_2(m)$. The procedure is repeated until PBR is evaluated for all the pixels in the $bCPM_2$. Next, the final $bCPM_2$ is used as a static mask, and $bCPM_1$ is optimized using the DBSA. Upon complete scan of the two bCPM, this approach produces a reconstructed image with an improved PBR relative to the initial bCPMs, and as reflected from the experiment, the final bCPMs yield higher SNR than the multilevel CPMs obtained from the GSA.

Even though the above process seems direct, it is complicated and slow. Calculating the intensity on the sensor plane due to a change of a single CPM pixel requires a convolution operation performed by an inverse Fourier transform of the product between the Fourier transform of the quadratic phase and the Fourier transform of the CPM. Overall, three Fourier transforms are needed [27] for every change of a CPM pixel. Every Fourier transform is implemented by a discrete Fourier transform (DFT) which requires $N \times N$ multiplications and additions. Hence the computation time increases proportionally to $3N^2$. After the development of the Cooley-Tukey algorithm [28], commonly known as fast Fourier transform (FFT), the number of operations is reduced from N^2 to $N\log(N)$. Therefore, each iteration consists of $3N\log(N)$, and a total of $3N^3\log(N)$ is necessary to complete one scan of the bCPM. Therefore, the above procedure is not computationally efficient compared to the procedure proposed next.

Table 1
The computational time for synthesizing the bCPMs with different matrix sizes.

Matrix size of bCPMs	Computational time (in seconds) for synthesizing bCPM	
	FFT-based DBSA	Fast DBSA method
100 × 100	102.09	36.89
200 × 200	1571.84	302.62
300 × 300	7469.62	5054.48
400 × 400	43,251.90	12,073.79
500 × 500	64,285.36	16,973.45

The total intensity on the sensor plane is the sum of the individual optical fields reaching the sensor plane from each pixel in the CPM plane. Therefore, the complex amplitude on the sensor plane in the m iteration due to flipping a CPM pixel at (X,Y) is

$$C_m(x,y) = C_{m-1}(x,y) \pm B_o \exp\left[i\frac{\pi}{\lambda z}\left\{(x-X)^2 + (y-Y)^2\right\}\right] \quad (9)$$

where B_o is a constant and the sign + or - is chosen according to the direction of change in the pixel value from 0 to 0.6π or vice versa. Based on Eq. (9), we propose to run the DBSA according to Eqs. (4), (7)-(9). For each m iteration, the CPM pixel at (X,Y) is flipped and the current complex amplitude $C_m(x,y)$ is updated according to Eq. (9). One of the intensities of Eq. (4) is updated as $|C_m(x,y)|^2$, and the new PSH is introduced into Eq. (7). Next, the new PBR is calculated by Eq. (8) and compared with the previous PBR. If the new PBR is higher than the previous one, the algorithm moves to flip the next pixel of the bCPM. Otherwise, the current pixel is flipped back to its previous value before toggling the next pixel. The DBSA was carried out for a matrix size of 500 × 500 pixels with M = 250,000 iterations. The PBR variation for M = 250,000 in steps of 10,000 iterations is shown in Fig 3(a). The PBR variation obtained by the FFT-based DBSA is depicted in Fig 3(b). The computational time of the proposed DBSA is compared with the time of FFT-based DBSA in Table 1. The computer used in this experiment for synthesizing the bCPMs had a 64-bit Intel(R) Core(TM) i7 microprocessor with a CPU clock rate of 3.40 GHz and installed memory (RAM) of 8.00 GB.

3. Experiments

The characteristics of LI-COACH with bCPMs synthesized using DBSA with two illumination channels are demonstrated using a digital holographic setup shown in Fig 4. The GSA is executed with 20 iterations, and the resulting CPM is binarized to obtain the initial guess of the

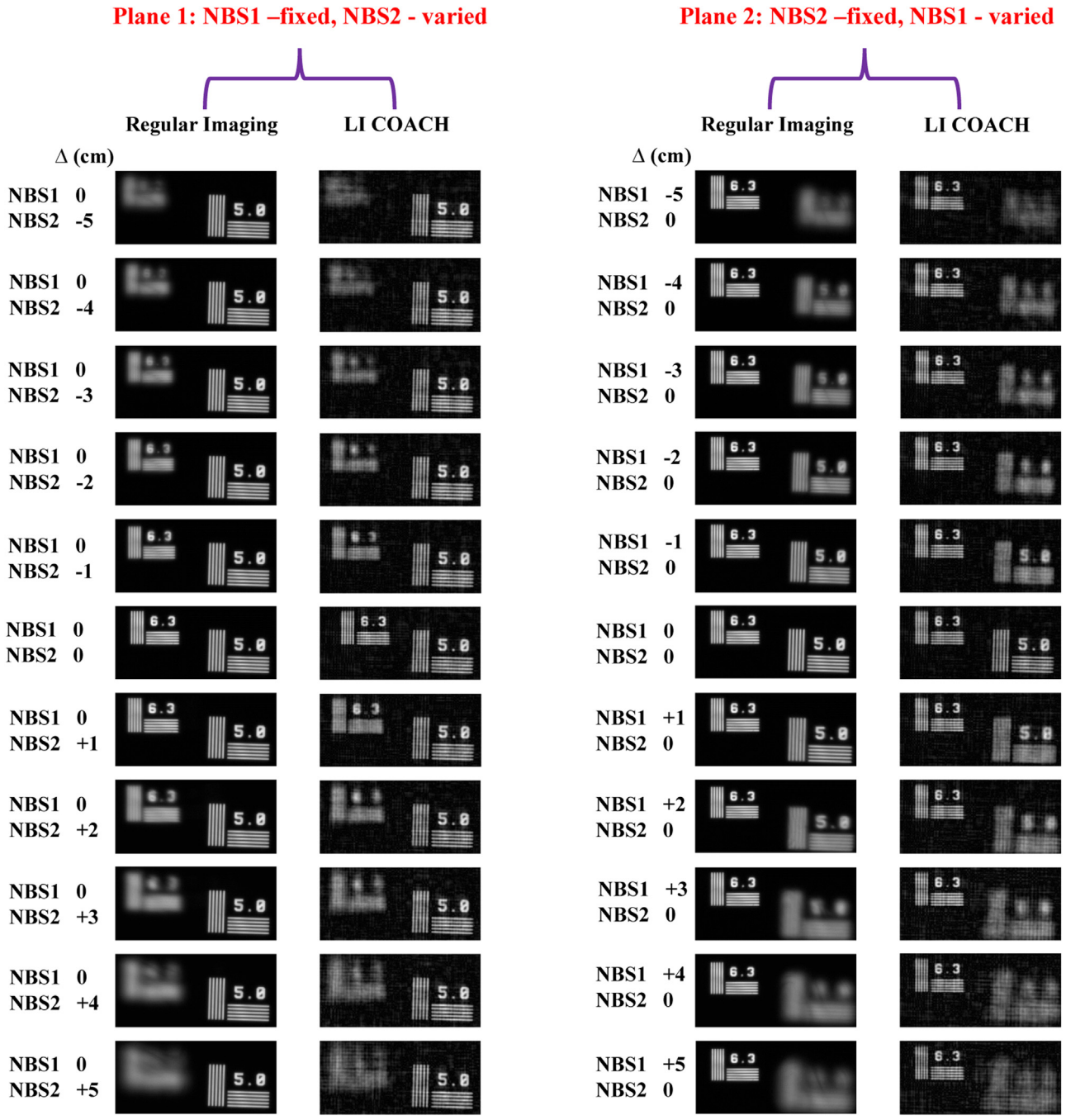

Fig. 7. Experimental comparison results of regular imaging and bCPM-based LI-COACH with holograms recorded for a two-plane object made up of two NBS RCs: NBS1 (element 5.0 *lp/mm*) in channel 1 and NBS2 RC (element 6.3 *lp/mm*) in channel 2. Image size is 941 × 421 pixels^2.

bCPM. Then the DBSA is executed N^2 times to obtain the final bCPM, where the size of the CPM matrix is $N \times N$ pixels. Both GSA and DBSA were executed a second time to synthesize the second bCPM. The experimental setup consists of two identical light-emitting diodes (LEDs) (Thorlabs LED635L, 170 mW, λ = 635 nm, $\Delta\lambda$ = 15 nm) mounted on two illumination channels. Two identical lenses, *L*1 and *L*2, were used to critically illuminate the objects: two negative National Bureau of Standards (NBS) (NBS 1963A Thorlabs) resolution charts (RCs) mounted in channel 1 and channel 2, respectively. In channel 1, element 5.0 *lp/mm* of NBS1 RC and in channel 2, element 6.3 *lp/mm* of NBS2 RC were critically illuminated. The distance between the lenses (*L*1 and *L*2) and the respective objects is 18 cm. A beam splitter BS1 is used to combine the light diffracted by the two objects (NBS1 and NBS2 RCs) and a polarizer, *P*, oriented along the active axis of SLM (Holoeye PLUTO, 1920 × 1080 pixels, 8 μm pixel pitch, phase-only modulation), is used after the BS1 to enable full modulation of the incident light. To control the *NA*, an iris with a radius of 0.8 cm was mounted just before the SLM. The *NA* of the illumination system is approximately 0.0125 ($NA=D/2z_s$, where D is the diameter of the aperture D = 0.8 cm; z_s=32 cm). The minimum resolved size of the system is about 31 μm ($0.61\lambda/NA$), and the minimal resolved length is 8 mm [$2\lambda/(NA)^2$]. Two bCPMs generated from two different initial random phase masks and computed by GSA and DBSA were displayed on the SLM, on an area of 1080 × 1080 pixels, one after the other. The two corresponding intensity patterns are recorded by a CMOS cam-

era [pco.edge 5.5 scientific CMOS (sCMOS), 2560 × 2160 pixels, 6.5 μm pixel pitch]. The camera is mounted at a distance of z_h=20 cm from the SLM. A pinhole with a diameter of ~80 μm was used as the point object in channel 1.

In the first experiment, two different bCPMs were synthesized and displayed on the SLM. The corresponding intensity patterns (I_{PSH1} and I_{PSH2}) were recorded by using the pinhole mounted at the back focal plane of the lens $L1$ while channel 2 was blocked. These recorded intensity patterns were subtracted one from the other to synthesize H_{PSH}. The pinhole was replaced by element 5.0 *lp/mm* of NBS1 RC and again, two intensity patterns (I_{OBJ1} and I_{OBJ2}) corresponding to the two bCPMs were recorded and subtracted one from the other to generate the object hologram H_{OBJ}. The image of the object was reconstructed by a cross-correlation between H_{OBJ} and the phase-only filtered version of H_{PSH}. As mentioned above, the phase-only filtering technique was implemented to reduce the background noise and to improve the SNR in the reconstructed image [13]. Figs. 5(a) and 5(b) show the bCPMs generated by the modified GSA and DBSA. The intensity patterns recorded using these bCPMs for the pinhole (I_{PSH1} and I_{PSH2}) and the NBS1 RC (I_{OBJ1} and I_{OBJ2}) are shown in Figs. 5(c)–5(d) and Figs. 5(e)–5(f), respectively. The images of PSH (H_{PSH}) and the object hologram (H_{OBJ}) are shown in Figs. 5(g) and 5(h), respectively. The reconstructed image of the object (NBS1 RC, element 5.0 *lp/mm*) with SNR=25.501 is shown in Fig 5(i). Fig. 5(j) shows the regular imaging of the same object. In order to test the performance of DBSA, the experiment was repeated for the bCPMs and multi-level CPM synthesized only by the GSA algorithm without the DBSA. The reconstructed images of the same object, in the cases of bCPMs and CPMs, are shown in Figs. 5(k) and 5(l), respectively. The SNRs of Figs. 5(k) and 5(l) are 6.618 and 15.213, respectively.

The phase sensitivity of DBS was studied by varying the phase value of the bCPM after synthesizing them by the DBSA. It was found that the reconstructed images are highly sensitive to the phase value of the bCPM. The reconstruction results with an error of $\pm\Delta\Phi = 0.2\pi$ are shown in Fig 6, which corresponds to a wavelength error of $\Delta\lambda \approx \pm$ 60 nm.

In the following experiment, the 3D imaging capabilities of the LI-COACH with bCPMs are demonstrated. First, a PSH library was created by moving the pinhole to all possible axial locations, Δ = −5 cm to +5 cm, in steps of 1 cm, centered on the back focal plane of the lens $L1$. Afterward, NBS1 RC was mounted in channel 1 and NBS2 RC on channel 2 and aligned in such a way that the elements of both the RCs were imaged without lateral overlap onto the sensor. Two planar objects with a different gap between them can be realized by varying the relative axial distance between the objects. The location of NBS1 RC was fixed, while the location of NBS2 RC was varied from −5 cm to +5 cm, in steps of 1 cm, about the back focal plane of the lens $L2$. At each location, two intensity patterns corresponding to the two bCPMs were recorded and subtracted one from the other to generate an object hologram. Different planes of the object (element 6.3 *lp/mm* of NBS2 RC) were reconstructed by correlating the object hologram with corresponding prerecorded PSHs. Similarly, the experiment was repeated in which NBS2 RC was fixed at the back focal plane of the lens $L2$, while the location of NBS1 RC was varied from −5 cm to +5 cm, in steps of 1 cm, about the back focal plane of the lens $L1$. The object holograms at each location were created and the different planes of the element 5.0 *lp/mm* of NBS1 RC were reconstructed by correlating the corresponding prerecorded PSHs. The reconstruction results of LI-COACH for the two-plane object and corresponding regular imaging results are shown in Fig 7. These results demonstrate that LI-COACH equipped with binary phase masks can perform 3D imaging, and when the bCPMs are synthesized with DBSA, the SNR is enhanced relative to masks synthesized by GSA alone.

4. Summary and conclusion

In conclusion, we have developed an algorithm of direct binary search for synthesizing binary phase masks for the imaging system of LI-COACH, enabling the use of the system in electromagnetic regions where multi-level phases cannot be implemented, such as X-rays, Gamma rays, and Terahertz. In the optics range, the proposed technique can be effective for a single shot COACH [29] equipped with a static binary mask that is fabricated by a photolithographic process. Binary masks are cheaper and simpler than multi-level masks, and their light modulation is more accurate.

There are several directions for future research with the proposed DBSA. The recent improvements of COACH can be integrated into the DBSA and by that to enhance the improvements of each technique. For example, the nonlinear image reconstruction proposed in [30,31] can replace the linear correlations of Eqs. (6) and (7). Consequently, a further improvement in the SNR is expected. Another improving development in COACH is the shape of the PSH, such as sparse dots [32] or rings [33]. These shapes are achieved by the modified GSA, where the specific PSH shape is the magnitude constraint on the camera plane. Since the initial stage of the DBSA is also GSA, we do not expect any difficulty in enforcing different magnitude constraints on the initial GSA and then continuing to the DBSA with the desired PSH form.

The current study demonstrates that the GSA used in most of the previous projects of COACH does not yield the optimal phase masks in the sense of maximum SNR for the reconstructed image. Therefore, other optimization algorithms with the same or other cost functions for binary or multilevel CPMs might improve the performance of the COACH family in the future.

Declaration of Competing Interest

The authors declare that they have no known competing financial interests or personal relationships that could have appeared to influence the work reported in this paper.

Data availability

The data that support the findings of this study are available from the corresponding author upon reasonable request.

Funding

V. A. acknowledges the European Union's Horizon 2020 research and innovation program grant agreement No. 857627 (CIPHR).

References

[1] Indebetouw G, Klysubun P, Kim T, Poon T-C. Imaging properties of scanning holographic microscopy. J Opt Soc Am A 2000;17(3):380–90.
[2] Rosen J, Brooker G. Digital spatially incoherent Fresnel holography. Opt Lett 2007;32(8):912–14.
[3] Rosen J, Brooker G, Indebetouw G, Shaked NT. A review of incoherent digital Fresnel holography. J Hologr Speckle 2009;5(2):124–40.
[4] Kim MK. Adaptive optics by incoherent digital holography. Opt Lett 2012;37(13):2694–6.
[5] Hong J, Kim MK. Single-shot self-interference incoherent digital holography using off-axis configuration. Opt Lett 2013;38(23):5196–9.
[6] Yanagawa T, Abe R, Hayasaki Y. Three-dimensional mapping of fluorescent nanoparticles using incoherent digital holography. Opt Lett 2015;40(14):3312–15.
[7] Oliver BM. Sparkling spots and random diffraction. Proc IEEE Lett 1963;51(1):220–1.
[8] Considine PS. Effects of Coherence on Imaging Systems. J Opt Soc Am 1966;56(8):1001–9.
[9] Mills JP, Thompson BJ. Effect of aberrations and apodization on the performance of coherent optical systems. II. Imaging. J Opt Soc Am A 1986;3(5):704–16.
[10] Rosen J, Brooker G. Non-scanning motionless fluorescence three-dimensional holographic microscopy. Nat Photonics 2008;2:190–5.
[11] Rosen J, Siegel N, Brooker G. Theoretical and experimental demonstration of resolution beyond the Rayleigh limit by FINCH fluorescence microscopic imaging. Opt Express 2011;19(27):26249–68.
[12] Vijayakumar A, Kashter Y, Kelner R, Rosen J. Coded aperture correlation holography-a new type of incoherent digital holograms. Opt Express 2016;24(11):12430–41.
[13] Vijayakumar A, Kashter Y, Kelner R, Rosen J. Coded aperture correlation holography (COACH) system with improved performance[Invited]. Appl Opt 2017;56(13):F67–77.

[14] Vijayakumar A, Rosen J. Spectrum and space resolved 4D imaging by coded aperture correlation holography (COACH) with diffractive objective lens. Opt Lett 2017;42(5):947–50.
[15] Vijayakumar A, Rosen J. Interferenceless coded aperture correlation holography – A new technique for recording incoherent digital holograms without wave interference. Opt Express 2017;25(12):13883–96.
[16] Kumar M, Vijayakumar A, Rosen J. Incoherent digital holograms acquired by interferenceless coded aperture correlation holography system without refractive lenses. Sci Rep 2017;7:11555.
[17] Feroci M, Costa E, Soffitta P, Del Monte E, Di Persio G, Donnarumma I, Evangelista Y, Frutti M, Lapshov I, Lazzarotto F, Mastropietro M, Morelli E, Pacciani L, Porrovecchio G, Rapisarda M, Rubini A, Tavani M, Argan A. SuperAGILE: the hard X-ray imager for the AGILE space mission. Nucl Instrum Methods Phys Res Sect A Accel Spectrom Detect Assoc Equip 2007;581(3):728–54.
[18] Alnafea M, Wells K, Spyrou NM, Saripan MI, Guy M, Hinton P. Preliminary results from a Monte Carlo study of breast tumour imaging with low-energy high-resolution collimator and a modified uniformly-redundant array coded aperture. Nucl Instrum Methods Phys Res Sect A Accel Spectrom Detect Assoc Equip 2006;563(1):146–9.
[19] Faust AA, Rothschild RE, Leblanc P, McFee JE. Development of a coded aperture X-Ray backscatter imager for explosive device detection. IEEE Trans Nucl Sci 2009;56(1):299–307.
[20] Damato AL, Horn BKP, Lanza RC. Coded source imaging for neutrons and X-rays. IEEE Nucl Sci Sympos Conf Rec 2007;1:199–2003.
[21] Seldowitz MA, Allebach JP, Sweeney DW. Synthesis of digital holograms by direct binary search. Appl Opt 1987;26(14):2788–98.
[22] Jennison BK, Allebach JP, Sweeney DW. Iterative approaches to computer-generated holography. Opt Eng 1989;28(6):629–37.
[23] Jennison BK, Allebach JP. Efficient design of direct-binary-search computer-generated holograms. J Opt Soc Am A 1991;8(4):652–60.
[24] Leportier T, Park MC, Kim YS, Kim T. Converting optical scanning holograms of real objects to binary Fourier holograms using an iterative direct binary search algorithm. Opt Express 2015;23(3):3403–11.
[25] Leportier T, Park M-C. Generation of binary holograms for deep scenes captured with a camera and a depth sensor. Opt Eng 2017;56(1):013107.
[26] Gerchberg RW, Saxton WO. A practical algorithm for the determination of phase from image and diffraction plane pictures. Optik 1972;35(2):227–46.
[27] Goodman JW. Introduction to fourier optics. New York: McGraw-Hill; 1968. p. 5–10.
[28] Cooley JW, Tukey JW. An algorithm for the machine calculation of complex Fourier series. Math Comput 1965;19:297–301.
[29] Rai MR, Vijayakumar A, Rosen J. Single camera shot interferenceless coded aperture correlation holography. Opt Lett 2017;42(19):3992–5.
[30] Rai MR, Vijayakumar A, Rosen J. Non-linear adaptive three-dimensional imaging with interferenceless coded aperture correlation holography (I-COACH). Opt Express 2018;26(14):18143–54.
[31] Liu C, Man T, Wan Y. Optimized reconstruction with noise suppression for interferenceless coded aperture correlation holography. Appl Opt 2020;59(6):1769–74.
[32] Rai MR, Rosen J. Noise suppression by controlling the sparsity of the point spread function in interferenceless coded aperture correlation holography (I-COACH). Opt Express 2019;27(17):24311–23.
[33] Liu C, Man T, Wan Y. High-quality interferenceless coded aperture correlation holography with optimized high SNR holograms. Appl Opt 2022;61(3):661–8.